Available online at www.sciencedirect.com
SCIENCE DIRECT®
Catalysis Today 96 (2004) 223–234
CATALYSIS TODAY
www.elsevier.com/locate/cattod

Catalyst performance for noble metal catalysed alcohol oxidation: reaction-engineering modelling and experiments

V.R. Gangwal, J. van der Schaaf, B.F.M. Kuster, J.C. Schouten*

Department of Chemical Engineering and Chemistry, Laboratory of Chemical Reactor Engineering, Eindhoven University of Technology, P.O. Box 513, 5600 MB Eindhoven, The Netherlands

Abstract

A reaction-engineering model is presented, which describes catalyst performance as a function of the catalyst activity profile, the reaction kinetics, and the degree of catalyst deactivation. With this model, the catalyst activity profile can be optimised for Pt catalysed methyl α-D-glucopyranoside (slowly-reactive) and glucose (highly-reactive) oxidations. This is done by comparing modelling results with experimentally obtained data for catalysts of different activity distributions. Experiments in a semi-batch stirred reactor showed that for methyl α-D-glucopyranoside (MGP) oxidation at oxygen partial pressures below 40 kPa, egg shell catalytic activity distribution gives a higher rate of oxidation than a uniform distribution. It was also observed that with increase in oxygen concentration from 10 to 40 kPa, the rate of deactivation due to catalyst over-oxidation increased dramatically. For glucose oxidation, both catalyst activity distributions give the same oxidation rate for all investigated oxygen partial pressures (5–100 kPa). The developed model adequately describes the observed experimental results of both reactions. It was found that the active metal particle size has a significant influence on the catalyst deactivation for MGP oxidation; the uniform catalyst with higher dispersion shows a higher deactivation rate than the egg shell catalyst. For modelling glucose oxidation, the effect of catalyst particle-to-bubble adhesion and higher diffusivity or partition coefficient for oxygen have to be taken into account.

Keywords: Catalyst activity distribution; Electrochemical kinetic model; Oxygen mass transfer; Reactor modelling; Catalyst potential; Overoxidation

1. Introduction

Noble metal catalysed selective oxidation of alcohols with molecular oxygen is an attractive process. It proceeds at rather mild reaction conditions, typically at temperatures below 90 °C and at atmospheric pressure, in neutral or slightly alkaline aqueous media. It has a major advantage of using a relatively cheap and environmentally friendly oxidant, as against traditional stoichiometric oxidations, which are based on expensive inorganic oxidants and yield large amount of toxic waste.

The noble metal catalysed alcohol oxidation has been extensively studied for a long time; review papers of Mallat and Baiker [1], Gallezot [2], and Kluytmans et al. [3] offer a useful survey of the subject. It is generally accepted that reaction takes place via a dehydrogenation mechanism followed by the oxidation of the adsorbed hydrogen atom with dissociatively adsorbed oxygen. The nature of catalyst deactivation is largely influenced by the amount of oxygen present at the catalytic surface. Several types of catalyst deactivation mechanisms have been identified, viz. over-oxidation, carbonaceous deposits, metal particle-growth, metal leaching, and chemical poisoning [4]. These deactivation mechanisms lead to a decrease of the active metal surface area and hence to a decrease of the reaction rate. It is known that over-oxidation is the most critical and predominant deactivation of all the types, which is also considered to be a main cause of catalyst deactivation in this study.

Extensive work has also been done in the field of electrochemistry on alcohol oxidation, but it is more focused on fuel cell applications as methanol oxidation. A detailed mechanism through which electro-oxidation of methanol

* Corresponding author. Tel.: +31 40 2473088; fax: +31 40 2446653.
E-mail address: J.C.Schouten@tue.nl, J.C.Schouten

0920-5861/$ – see front matter © 2004 Elsevier B.V. All rights reserved.
doi:10.1016/j.cattod.2004.06.146

Nomenclature

a	surface area of the gas–liquid and liquid–solid film (m^{-1})
C_{cat}	catalyst concentration (kg m^{-3})
C_{ls}	concentration at the liquid side of liquid–solid interface (mol m^{-3})
C_{MGP}	MGP concentration (mol m^{-3})
C_{MAGP}	MAGP concentration (mol m^{-3})
C_{MG}	MG, product concentration (mol m^{-3})
C	oxygen concentration in the particle (mol m^{-3})
C_{sat}	equilibrium oxygen concentration in the liquid (mol m^{-3})
C_L	oxygen concentration in the bulk liquid (mol $m-^{3}$)
C_S	oxygen concentration at the catalyst surface (mol m^{-3})
D_e	effective diffusivity (m^2 s^{-1})
E	catalyst potential (V)
F	Faraday's constant (C mol^{-1})
$F_{V,G}$	volumetric gas flow rate (m^3 s^{-1})
k_i	defined in Table 2
K_i	equilibrium rate constants, in Table 2
K_{GL}	gas-to-liquid mass transfer coefficient (m s^{-1})
k_{LS}	liquid-to-solid mass transfer coefficient (m s^{-1})
l	diffusion path length (m)
L_t	weight specific catalyst surface (mol kg_{cat}^{-1})
P	oxygen partial pressure inside the reactor (kPa)
R	gas constant (J mol^{-1} k^{-1})
R_i	reaction rate of species i (Table 1)
R_{RCH_2OH}	specific reaction rate of alcohol (mol kg^{-1} s^{-1})
R_{RCHO}	specific reaction rate of aldehyde (mol kg^{-1} s^{-1})
R_{v,O_2}	volumetric reaction rate of oxygen (mol m^{-3} s^{-1})
t	time (s)
T	temperature (K)
V	volume (m^3)
x	distance inside the catalyst particle (m)
*	free adsorption site
$*_\rho$	free adsorption site for organic compound
$*_s$	free site for oxide formation

Greek letters

ε	porosity
ρ	density (kg m^{-3})
τ	tortuosity
Θ	surface coverage

Subscripts

cat	catalyst
e	effective
H^+	proton ion
G	bulk gas
L	bulk liquid
GL	gas–liquid
LS	liquid–solid
p	catalyst particle
V	volume

Abbreviations

C	Carbon
Gr	Graphite
MAGP	methyl α-D-6-aldehydo-glucopyranoside
MG	1-*O*-methyl α-D-glucuronic acid
MGP	methyl α-D-glucopyranoside or methyl glucoside
RCH_2OH	alcohol compound
RCHO	aldehyde compound
RCOOH	acid compound

occurs seems to be generally accepted [5]. For higher aliphatic alcohols, the mechanism is more complex due to increased variation in terms of intermediates and products, so different electro-oxidation mechanisms have been proposed [5,6].

According to Horanyi [7] and Mallat and Baiker [1], noble metal catalysed oxidations can be considered as electrochemical reactions. For example, alcohol oxidation takes place in two half reactions: alcohol dehydrogenation (producing electrons and protons) and oxygen reduction (consuming electrons and protons). Based on this principle Markusse et al. [8] have developed a kinetic model, which uses the electrochemical potential of the catalyst to describe the experimentally observed data in the heterogeneous catalytic system. However, this model was only based on intrinsic kinetic data. Gangwal et al. [9] explored the model rigorously by including oxygen mass transport limitation. It was found that the catalytic active site distribution has a strong influence on the catalyst performance. The present work deals with an experimental study on the effect of active site distributions, viz. egg shell and uniform, on the catalyst performance. The goal is to develop a reaction-engineering model for alcohol oxidation, which describe catalyst performance as a function of the catalyst activity profile, the reaction kinetics, and the degree of catalyst deactivation. Pt catalysed oxidation of methyl α-D-glucopyranoside (MGP), a low chemical reactivity compound, and of glucose, a high chemical reactivity compound, were used as test reactions. The stoichiometry of the reactions is shown in Fig. 1.

2. Reaction-engineering model

This work uses the electrochemical kinetic model developed by Markusse et al. [8]. According to this model,

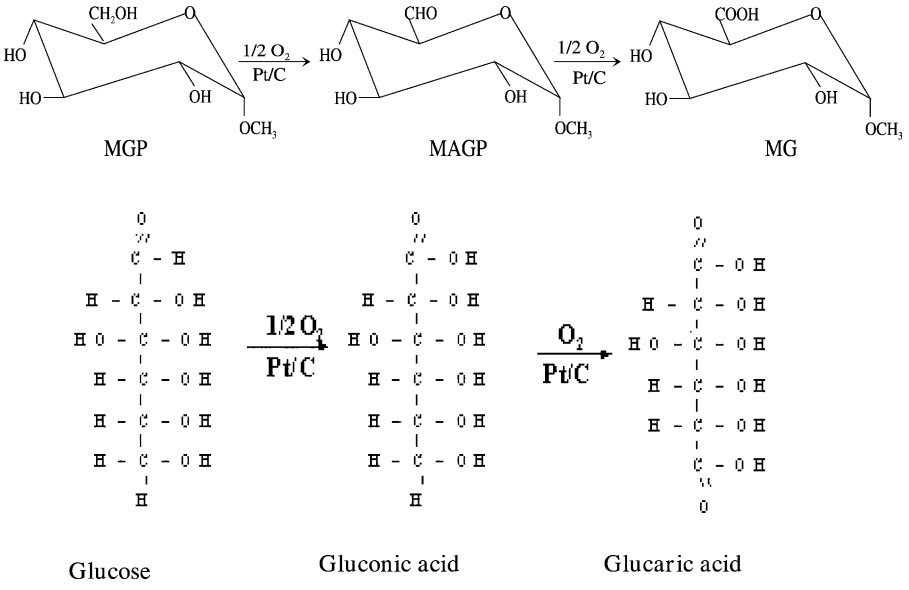

Fig. 1. Reactions under investigation.

with increase in oxygen concentration, the electrochemical potential of the catalyst increases, which leads to an increase in the oxidation rate as well as to catalyst deactivation due to over-oxidation. The electrochemical kinetic model is presented in Table 1, a detailed description is given elsewhere [9]. It was found that for the methyl α-D-glucopyranoside oxidation a new set of kinetic parameters improved the performance of the kinetic model, now being suited for intrinsic kinetic as well as for mass transport limited conditions [10]. The new kinetic parameters are presented in Table 2.

For the reaction to take place, oxygen has to be transferred from the gas phase to the liquid phase, through the liquid to the catalyst particle, and finally has to diffuse through the pores to the catalytic site inside the particle, as shown in Fig. 2. The assumptions used for deriving the model are:

1 The system is isothermal and heat effects are negligible.

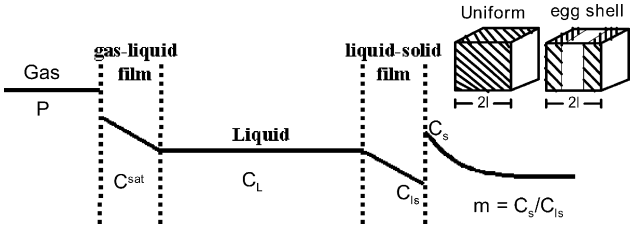

Fig. 2. Oxygen mass transfer in a stirred slurry reactor.

2 No concentration gradients for the alcohol reactant; at the liquid–solid film and inside the catalyst particle.
3 The catalyst particles are flat plate with constant shape and porosity.

The transient material balance equations for oxygen, in the gas phase, the liquid phase and the solid phase are discussed consecutively.

Table 1
Reaction mechanism for the alcohol oxidation, with rate equations (Markusse et al., 2001)

Reaction	Rate equation	
O_2+2*→2O*	$R_1 = k_1 C_{O_2} \Theta *^2$	(I)
$RCH_2OH + *_\rho \rightleftharpoons RCH_2OH *_\rho$	$\Theta_{RCH_2OH} = K_2 C_{RCH_2OH} \Theta *_\rho$	(II)
$RCHO + *\rho \rightleftharpoons RCHO * \rho$	$\Theta_{RCHO} = K_2 a C_{RCHO} \Theta *_\rho$	(IIa)
$RCH_2OH *_\rho + * \rightarrow RCHO *_\rho + 2H^+ + 2e^- + *$	$R_3 = k_3 \Theta_{RCH_2OH} \Theta * \exp(EF/RT)$	(III)
$RCHO *_\rho + * \rightarrow RCOOH *_\rho + 2H^+ + 2e^- + *$	$R_4 = k_4 \Theta_{RCHO} \Theta * \exp(EF/RT)$	(IV)
$O* + H^+ + 2e^- \rightarrow OH^- + *$	$R_5 = k_5 C_H + \Theta_O exp(-EF/RT)$	(V)
$O* + *_s \rightarrow Ox *_s + *$	$R_6 = k_6 \Theta_O (1 - \Theta_{ox})$	(VI)
$RCOOH *_\rho + NaOH \rightleftharpoons RCOONa + * \rho + H_2O$	$\Theta_{RCOOH} = K_7 C_{RCOOH} \Theta *_\rho$	(VII)
$Ox *_s + H^+ + 2e^- + * \rightarrow OH^- + * + *_s$	$R_8 = k_8 C_{H_+} \Theta_{ox} \Theta * \exp(-EF/RT)$	(VIII)

Table 2
List of values of kinetic parameters

Symbol	Description	Old parameters Pt/Gr [8,9]	New parameters Pt/Gr [10]	Adopted Pt/carbon
k_1 ($m^3\ mol^{-1}\ s^{-1}$)	Oxygen adsorption rate constant	6.5×10^3	9.3×10^{-1}	9.3×10^{-1}
k_2 ($m^3\ mol^{-1}$)	Alcohol adsorption constant	1.3×10^{-2}	2.0×10^{-3}	6.0×10^{-3}
k_{2a} ($m^3\ mol^{-1}$)	Aldehyde adsorption constant		2.0×10^{-3}	6.0×10^{-3}
k_3 (s^{-1})	Alcohol dehydrogenation constant			
	(a) MGP dehydrogenation constant	3.9×10^{-6}	4.5×10^{-8}	4.5×10^{-8}
	(b) Glucose dehydrogenation constant			2.1×10^{-6}
k_4 (s^{-1})	Aldehyde dehydrogenation constant			5.6×10^{-6}
k_5 ($m^3\ mol^{-1}\ s^{-1}$)	Oxygen reduction constant	3.5×10^{10}	1.2×10^{11}	1.2×10^{11}
k_6 (s^{-1})	Oxide formation constant	1.2×10^{-3}	1.2×10^{-3}	1.2×10^{-3}
k_7 ($m^3\ mol^{-1}$)	Acid adsorption constant	1.8×10^{-1}	5.0×10^{-2}	5.0×10^{-2}
k_8 ($m^3\ mol^{-1}\ s^{-1}$)	Oxide reduction constant	1.6×10^9	1.5×10^8	1.5×10^8

2.1. Gas phase (G) mass balance

Oxygen mass transport from the gas phase to the liquid phase:

$$\frac{V_G}{RT}\frac{dP}{dt} = F_{V,G}^{in}\frac{P^{in}}{RT} - F_{V,G}^{out}\frac{P}{RT} - k_{GL}a_{GL}V_L(C^{sat} - C_L) \quad (1)$$

where P is the oxygen partial pressure in the reactor, $k_{GL}aGL$ is the volumetric gas-to-liquid mass transport coefficient, C^{sat} is the saturation oxygen concentration, and C_L is the oxygen concentration in the liquid phase.

2.2. Liquid phase (L) mass balance

Oxygen mass transport from the liquid phase to the solid phase:

$$V_L\frac{dC_L}{dt} = k_{GL}a_{GL}V_L(C^{sat} - C_L) - k_{LS}a_{LS}V_L\left(C_L - \frac{C_s}{m}\right) \quad (2)$$

where $k_{LS}a_{LS}$ is the volumetric liquid-to-solid mass transport coefficient, and C_S is the oxygen concentration at the solid particle. The partition coefficient m is used to take into account the possibility that the oxygen concentration just within the surface of the solid, C_S, may be higher than the oxygen concentration in the liquid just adjacent to the solid, C_{lS}. Throughout the paper, it is assumed that the partition coefficient equals 1.

2.3. Solid phase (S)

It is assumed that active sites are located inside the pores of the catalyst particle. This is also necessary to be able to differentiate between catalyst of different intra particle activity distributions. For a uniformly activated flat plate catalyst particle and constant oxygen diffusivity, the oxygen balance under isothermal conditions leads to:

$$\frac{\partial C}{\partial t} = D_e\frac{\partial^2 C}{\partial x^2} - R_{v,o_2} \quad (3)$$

with the following initial and boundary conditions:

at $t = 0$

$$C = 0 (0 \le x \le l) \quad (4)$$

at $t > 0$:

$$\frac{dC}{dx} = 0, \quad \text{at} \quad x = 0 \quad (5)$$

$$\left(-D_e\frac{dC}{dx}\right) = k_{LS}\left(C_L - \frac{C_S}{m}\right), \quad \text{at}\, x = l \quad (6)$$

where C is oxygen concentration inside the catalyst particle, l is the diffusion path length, and D_e is the effective diffusivity for oxygen. The volumetric rate of reaction of oxygen R_{v,o_2}, is dependent on the amount of oxygen present at the catalyst surface as well as on the activity of the catalyst. Therefore, from Eq. (I) of Table 1,

$$R_{v,o_2} = L_t\rho_p k_1 \Theta *^2 C \quad (7)$$

The rate of reaction can also be expressed in terms of the specific consumption of reactant alcohol from Eq. (III) in Table 1 as:

$$R_{RCH_2OH} = L_t k_3 \Theta_{RCH_2OH}\Theta * \exp\left(\frac{EF}{RT}\right) \quad (8)$$

L_t is the specific number of platinum surface atoms, i.e. mol $Pt_s/kg_{catalyst}$, based on the assumption that one Pt surface atom equals one catalytic site. For the egg shell catalyst the given amount of active metal is distributed in the outer 20% of the volume of the flat plate particle.

2.4. Material balance for liquid reactant and products

The liquid reactant alcohol is in a batch mode and continuously converting to the product as reaction pro-

gresses; e.g. methyl glucoside (MGP) gives methyl glucuronic acid (MG) with methyl aldehydo-glucoside (MAGP) as an intermediate; whereas glucose, first gives gluconic acid, which further reacts to give glucaric acid, as shown in Fig. 1.

The rate of disappearance of MGP to aldehyde is

$$\frac{dC_{RCH_2OH}}{dt} = -C_{cat}R_{RCH_2OH} \quad (9)$$

Aldehyde is a highly reactive intermediate. It was found that at slightly acidic pH, the aldehyde content during MGP oxidation was never more 2% [11]. Additionally increasing pH (alkaline condition) leads to even higher rate of aldehyde disappearance [12]. The model developed here also shows a low aldehyde concentration of less than 1%. However, it is important to consider its formation and disappearance, in order to model the initial oxidation rate properly. It is given as:

$$\frac{dC_{RCHO}}{dt} = C_{cat}(R_{RCH_2OH} - R_{RCHO}) \quad (10)$$

where R_{RCHO} is the rate of aldehyde dehydrogenation and is determined from Eq. (IV), Table 1 as:

$$R_{RCHO} = L_t k_4 \Theta_{RCHO} \Theta * \exp\left(\frac{EF}{RT}\right) \quad (11)$$

where Θ_{RCHO} is aldehyde surface coverage and is calculated from Eq. (IIa) of Table 1. The adsorption constant of aldehyde is considered to be equal to that of reactant alcohol. The catalyst potential, E, is determined by balancing the rate of electrons produced ($2R_3 + 2R_4$) per volume of the catalyst and the rate of electrons consumed ($2R_5 + 2R_8$) per volume of the catalyst as:

$$E = \frac{RT}{2F}\ln\left(C_{H_+}\frac{< L_t\rho_p k_5\Theta_o > + < L_t\rho_p k_8\Theta_{ox}\Theta * >}{< L_t\rho_p k_3\Theta_{RCH_2OH}\Theta * > + < L_t\rho_p k_4\Theta_{RCHO}\Theta * >}\right) \quad (12)$$

where $< >$ denotes the averaged values.

The rate of acid formation is calculated from the rate of dehydrogenation of aldehyde as:

$$\frac{dC_{RCOOH}}{dt} = C_{cat}R_{RCHO} \quad (13)$$

During the reaction, as alkali (NaOH) is used for controlling the pH, the reactor liquid volume is changing with the reactant conversion. This also depends upon the concentration of alkali used. Therefore, the total volume is determined as follows:

$$V_L = \frac{V_{L,ini}}{(1 - C_{RCOOH}/C_{NaOH})} \quad (14)$$

where $V_{L,ini}$ is the initial liquid volume in the reactor, and V_L is the new volume of the reactor due to alkali addition.

For D-glucose oxidation, glucose is considered to be in aldehyde form. Therefore, the rate of disappearance of glucose is modelled through the rate of dehydrogenation of aldehyde (Eq. (11)) and the respective kinetic parameter is presented in Table 2. At kinetic limited conditions, glucose oxidation on Pt gives rise to a consecutive reaction, in which gluconic acid reacts further to give glucaric acid as shown in Fig. 1. However, the second reaction is slower than the first one and at low conversion (<30%) its influence on kinetics can be neglected. In this work, only the first step to gluconic acid is considered.

For modelling purpose, as the catalyst used in this study is Pt on active carbon support, in order to obtain the best fit, the alcohol adsorption constant (K_2) comes out to be three times higher than the one presented in Table 2 for the graphite support. Vleeming et al. [13] have thoroughly investigated the effect of catalyst supports and found that in case of methyl glucoside oxidation, the catalyst support has significant influence on the initial activity of the catalyst. According to Vleeming, the initial activity for the activated carbon support is three to four times higher than for the graphite support. This can be due to the interaction of the support groups with the alcohol molecule, which then determines the orientation of the hydroxyl groups of the alcohol compound towards the platinum surface and thus influences the adsorption of the alcohol on a platinum site. This can have a strong effect on turn over frequency [14].

The reactor model equations are solved with Matlab software. The ordinary differential Eqs. (1) and 2 are solved using ODE23s routine. For solving the partial differential equation (Eq. (3)), a second order finite difference method is used. The speed and accuracy of calculations are ensured through proper selection of the number of grid points (50) and the time step (0.05 s). The boundary condition (Eq. (6)) is solved using a three point forward finite difference method. The model simulations are performed with the adopted kinetic parameters for Pt on carbon (Pt/C) catalysts presented in Table 2 and parameters presented in Table 5.

3. Experimental

The experimental work is performed in a three phase semi-batch stirred slurry reactor. The reaction is carried out by keeping the aqueous alcohol reactant in batch mode and the gaseous oxidant (molecular oxygen) in continuous mode. The partial pressure of oxygen was the main operating variable, while all other operating conditions were remained constant during the experiments. An overview of the reaction conditions for the methyl α-D-glucopyranoside and glucose oxidation experiments is given in Table 3. It is to be noted that all the experimental results presented here are obtained at potentials higher than 0.4 V versus reversible hydrogen electrode (RHE), which supports the fact that the observed data are free from possible catalyst deactivation due to alcohol degradation products or decarbonylation, and that the observed catalyst deactivation is only caused by over-oxidation.

Table 3
Experimental conditions used for both the reactions

Condition	Range
Initial concentration (mol m^{-3})	100
Oxygen partial pressure (kPa)	5–100
Total pressure (kPa)	100
pH	8
Degree of conversion (%)	5–40
Temperature (K)	323
Catalyst particle size (μm)	40
Stirring speed (rpm)	1000

Table 4
Catalysts properties

Properties	Egg shell	Uniform
Pt loading (wt.%)	5	5
Dispersion (%)	42	58
BET surface area (cm^2/g)	900	900
Particle size distribution (μm)	7–120	7–120
Porosity (%)	80	80
L_t (mol $Pt/kg_{catalyst}$)	0.5384	0.1487

3.1. Catalysts

Pt on carbon catalysts with different activity distributions were obtained from Engelhard B.V., The Netherlands. The different activity distributions were uniform and edge coated (egg shell). The uniform catalyst distribution means that the Pt metal is evenly distributed inside the pores of the carbon particle. The edge coated (egg shell) distribution means that the Pt metal is located mainly at the outer part of the carbon particle. According to the manufacturer, catalysts have the same particle size distribution, Pt loading, and BET surface area, which is verified with our own measurements, the catalyst properties are given in Table 4.

In order to compare the different catalysts for their total catalytic activity, the Pt loading and the fraction of exposed atoms (dispersion) must be determined. The dispersions for the two types of the catalyst, as measured by CO chemisorption, are presented in Table 4. The uniform catalyst has a significantly higher dispersion than the egg shell catalyst.

3.2. Equipment and procedure

The oxidation is carried out in a reactor of 1000 ml volume. The glass reactor was equipped with a glass stirrer with internal gas circulation, a pH electrode (Radiometer PHC 2402), an oxygen electrode (Ingold 341003005), and a membrane filter of 0.45 μm (Millipore GVWP09050) to retain the catalyst sample. During the reaction the pH was kept constant automatically using a pH meter (Radiometer-PHM 82), a pH controller (Radiometer-TTT80), and a motor burette (Radiometer-ABU80, 25 ml) containing 0.1 M sodium hydroxide (NaOH) solution. The inlet gas flow was kept constant using Bronkhorst mass flow controllers. The oxygen concentration in the liquid was monitored using an oxygen electrode. The oxygen electrode displayed the percentage of equivalent saturation pressure of oxygen dissolved in the slurry. The temperature was measured with a Pt-100 probe and controlled by a water bath (Beun de Ronde CS6 and R22). The reactor was operated at atmospheric pressure.

The catalyst and 400 ml of water were introduced into the reactor. The reactor was flushed with 500 ml min^{-1} nitrogen flow and the catalyst slurry was stirred at 1000 rpm until it reached to 323 K. Aqueous reactant solution of 100 ml was then added to the reactor under the constant nitrogen flow of 500 ml min^{-1}. For the methyl α-D-glucopyranoside oxidation before adding the reactant solution to the reactor, the catalyst is reduced in a 125 ml min^{-1} hydrogen flow for about 30 min. In case of the glucose oxidation, the reactant solution was directly added to the reactor without reducing the catalyst as it is a strong reducing agent. The reactor content was then stirred until the desired reaction temperature was reached. As soon as the reaction temperature is attained, the pH control system was activated and pH is brought to the desired level. Before starting the reaction, the stirring speed was lowered to 600–700 rpm and oxygen was introduced in the reactor at the desired flow rate. The oxidation is started by setting the stirring speed to the original level of 1000 rpm. At the same time recording of all the signals viz., addition of NaOH, liquid oxygen concentration, and electrochemical potential, was activated. The rate of oxidation (acid product formation) is measured through addition of alkali. The reaction was carried out in an aqueous alkaline medium at constant pH and temperature.

Table 5
List of values of model parameters used in the simulations

Symbol	Description	Value	Comment or reference
ρ_p (kg m^{-3})	Particle density	1050	Carbon particle
D (m^2 s^{-1})	Oxygen diffusivity	3×10^{-9}	Perry et al. [21]
ε	Porosity	0.8	Mercury porosometry
τ	Tortuosity	2–4	Vleeming et al. [4]
D_e (m^2 s^{-1})	Effective oxygen diffusivity	1.2×10^{-9}	$\varepsilon D/\tau$
$k_{GL}a_{GL}$ [s^{-1}]	Gas-to-liquid mass transfer coefficient	0.4	Dynamic gas absorption [22]
k_{LS} (m s^{-1})	Liquid-to-solid mass transfer coefficient	1.2×10^{-3}	Sano et al. [23]
C_{H+} (mol m^{-3})	Proton concentration	1×10^{-5}	pH value of 8
T (K)	Temperature	323	Isothermal condition

3.3. Electrochemical measurement

The electrochemical Nernstian potential of the catalyst was measured using a smooth platinum wire, a Ag/AgCl, sat KCl (0.197 V standard potential) reference electrode hosted in a lugin capillary, and a millivolt (mV) meter. The Pt wire electrode was continuously contacted by the catalyst particles in the slurry reactor and thus attained the potential of the catalyst. This method is well established in metal catalyzed hydrogenation reactions and Mallat and Baiker [15,16] have effectively demonstrated its usefulness in alcohol oxidation. However, this method is affected by several factors like support conductivity, catalyst concentration, frequency and duration of collisions of particles, electrolyte resistance, substrate deposition on the electrode, adhering support particles, and electrochemical and geometrical area of the electrode. In spite of all these, with use of a low electrochemical surface area electrode (smooth Pt wire), sufficient catalyst concentration, high stirring speed, and using the reference electrode at close distance, makes this technique unique, in giving in situ on line information on the oxidation state of the catalyst.

4. Results and discussion

4.1. Methyl α-D-glucopyranoside oxidation

4.1.1. Effect of low oxygen partial pressure

Fig. 3a shows the acid formation rate as a function of time for the egg shell and the uniform catalyst at 10 kPa oxygen partial pressure. From the experimental observation, it can be seen that the egg shell catalyst shows a higher activity than the uniform catalyst. This also can be seen in Fig. 3b, where the concentration of methyl glucoside against time is presented. Here, the egg shell catalyst gives almost 1.5 times higher conversion than the uniform catalyst. The simulation results shown in Fig. 3a, indicate that the model adequately describes the initial observed rates for the egg shell catalyst. However, the model shows slightly faster deactivation than observed in the experiment. The catalyst deactivation can be seen through Fig. 3c, which shows the simulated oxide coverage against time. For the uniform catalyst, the model is well able to describe the observed rate. The possible explanation for the low performance of the uniform catalyst is that stronger oxygen concentration gradients are present inside the particle as compared to the egg shell catalyst, which lowers the effectiveness of the uniform catalyst.

Fig. 3d shows measured and calculated potentials as a function of time. It can be seen that starting from a reduced catalyst (0.1 V potential) surface, the catalyst potential instantly increases to 0.8 V, as soon as the oxygen reaches the catalyst surface. The catalyst potential stabilizes at a higher level of around 0.9 V. The developed model predicts the experimentally observed potential well for both catalysts. Although, the trend for the modelling results is opposite than measured in the experiments, it is not considered significant at the moment, in view of the limitations of the potential measurement method.

4.1.2. Effect of higher oxygen partial pressure

Fig. 4a shows the acid formation rate as a function of time for the egg shell and the uniform catalyst at 40 kPa oxygen partial pressure. The initial oxidation rate is almost a factor of two times higher for both catalysts than at 10 kPa oxygen partial pressure, but also the rate of deactivation due to over-oxidation is faster. It can also be seen from Fig. 4a that the egg shell catalyst gives a slightly higher initial rate of oxidation than the uniform catalyst, which is similar as for 10 kPa oxygen partial pressure. The results presented in Fig. 4a and 4b indicate that the model is well able to describe the experimentally observed high initial rate followed by faster deactivation, for both catalysts. However, for the uniform catalyst, the model predicts higher rates and less deactivation than observed in the experiment. This may be due to the fact that the simulations have been carried out considering similar Pt–oxygen bonding for both catalysts, i.e. the uniform catalyst with higher dispersion, results in higher activity.

In practice it has been found that the dispersion or Pt particle size, has a large influence on the Pt–oxygen bonding. X-ray photoelectron spectroscopy studies performed by Parmigiani et al. [17] revealed that platinum is more easily oxidized with decreasing particle size (higher dispersion). Schuurman et al. [11] have found a similar effect for the methyl glucoside oxidation. In order to verify these facts, simulations are performed using increased Pt–oxygen bonding. This is done simply by taking the oxide formation constant five times higher. The results in Fig. 4a show that the model performance has improved significantly and that the model describes the observed experimental rates and conversion accurately. Fig. 4c shows oxide formation as function of time, it can be seen that at 5000 s more than 60% of the active sites are covered with the oxide, which indicates how fast the deactivation is at higher oxygen concentration. Simulations are also performed using increased Pt–oxygen bonding for 10 kPa oxygen partial pressure. It was found that, not shown in Fig. 3a, the oxide coverage fraction increased by a factor of five, from 0.016 to 0.08, which decreases acid formation rate, less than 10%, i.e. considered to be insignificant. To understand the observed catalyst deactivation, catalyst potential against time is presented in Fig. 4d. It can be seen that starting from a reduced catalyst (0.1 V potential) surface, the catalyst potential instantly increases to 0.9 V as soon as the oxygen reaches the catalyst surface and stabilizes to a higher level around 0.97 V. This indicates that the catalyst is deactivated very fast, i.e. high oxide coverage, which is very well described by the model for both catalysts. Comparing Fig. 3d with 4d, although the difference of 0.9 and 0.97 V might seem small, it has a very

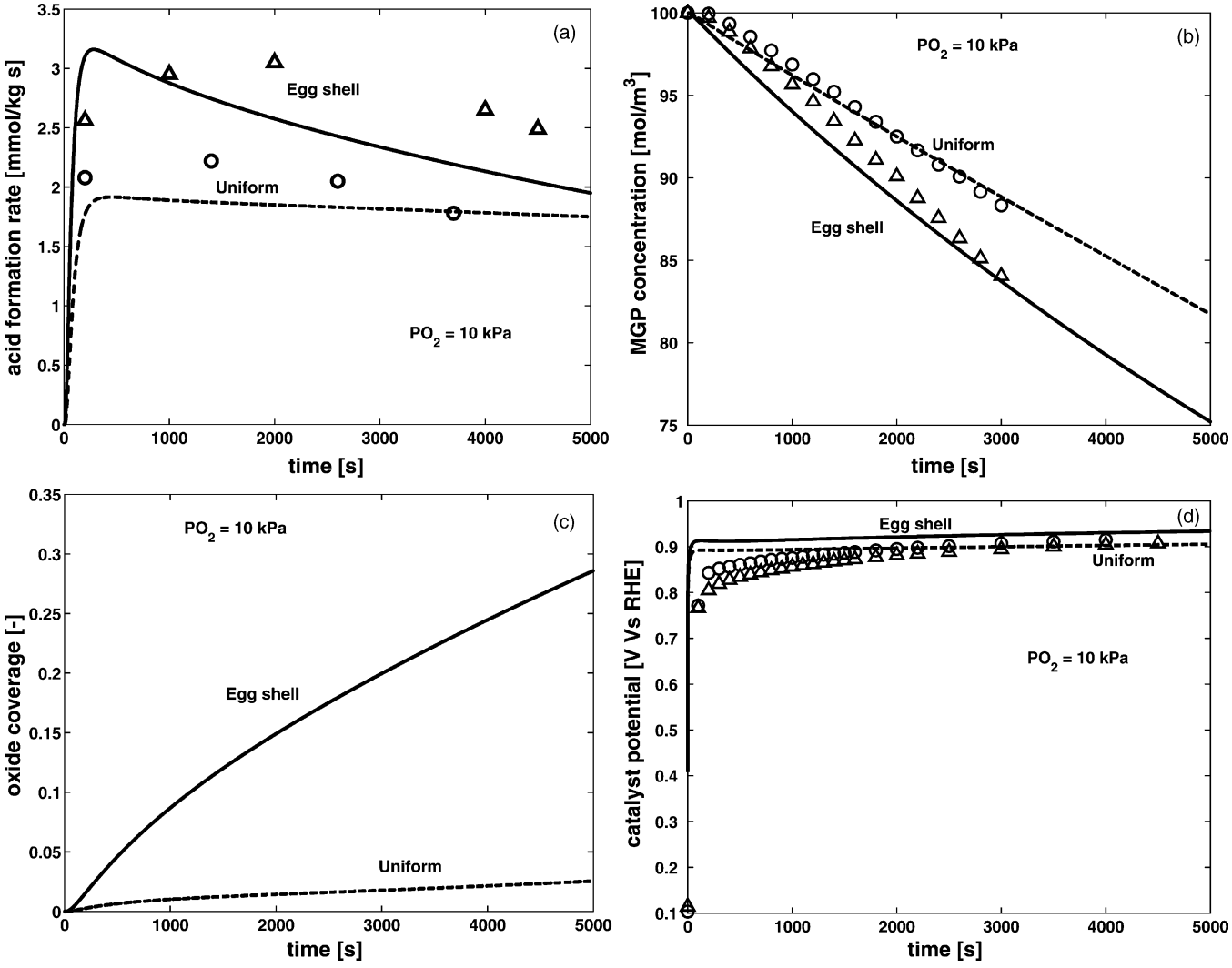

Fig. 3. MGP oxidation: the effect of a low oxygen partial pressure on the catalyst performance: (a) acid formation rate; (b) concentration of MGP; (c) fraction of the oxide coverage; and (d) in situ open-circuit catalyst potential. Symbols represent the experimental and continuous lines represent the modelling results. For the egg shell catalyst, triangles and solid lines are used, whereas for the uniform catalyst circles and dashed lines are used.

large effect on the catalyst deactivation, the oxide coverage becomes almost two times higher.

4.2. Glucose oxidation

4.2.1. Effect of low oxygen partial pressure

Fig. 5a shows the acid formation rate as a function of time for the egg shell and the uniform catalyst at 5 kPa oxygen partial pressure. It is clearly seen from the acid formation rate that both catalysts are active, and show no sign of deactivation. Experimental data show that the uniform catalyst gives a slightly higher oxidation rate. The model results presented in Fig. 5a, show that strong concentration gradients are present inside the particle for both catalysts, corresponding to lower oxidation rates than found experimentally. This deviation of the model might be caused by a fast reaction, like glucose oxidation on Pt/C catalyst, which mainly takes place at the gas–liquid interface [18,19]. The effect is even more pronounced if there is particle-gas bubble interaction, which has a significant influence on the liquid-to-solid mass transfer [20]. This phenomenon is termed as particle bubble adhesion (PBA).

So, taking above effects into account, simulations were performed with factor of five to ten times higher gas-to-liquid and liquid-to-solid mass transfer coefficients. The model performance did improve, but still large deviations from the observed experimental data was found. At a low oxygen concentration, egg shell catalysts are expected to perform better than uniform catalysts, which is not seen in the experiments. Possibly, the apparent oxygen diffusivity is higher than what is used so far. Alternatively, the distribution coefficient (m) for carbon support may be higher due to a high affinity for oxygen. To investigate the sensitivity to diffusivity and mass transfer coefficients, simulations are performed with a factor of ten times higher effective diffusivity and mass transfer coefficients than presented in

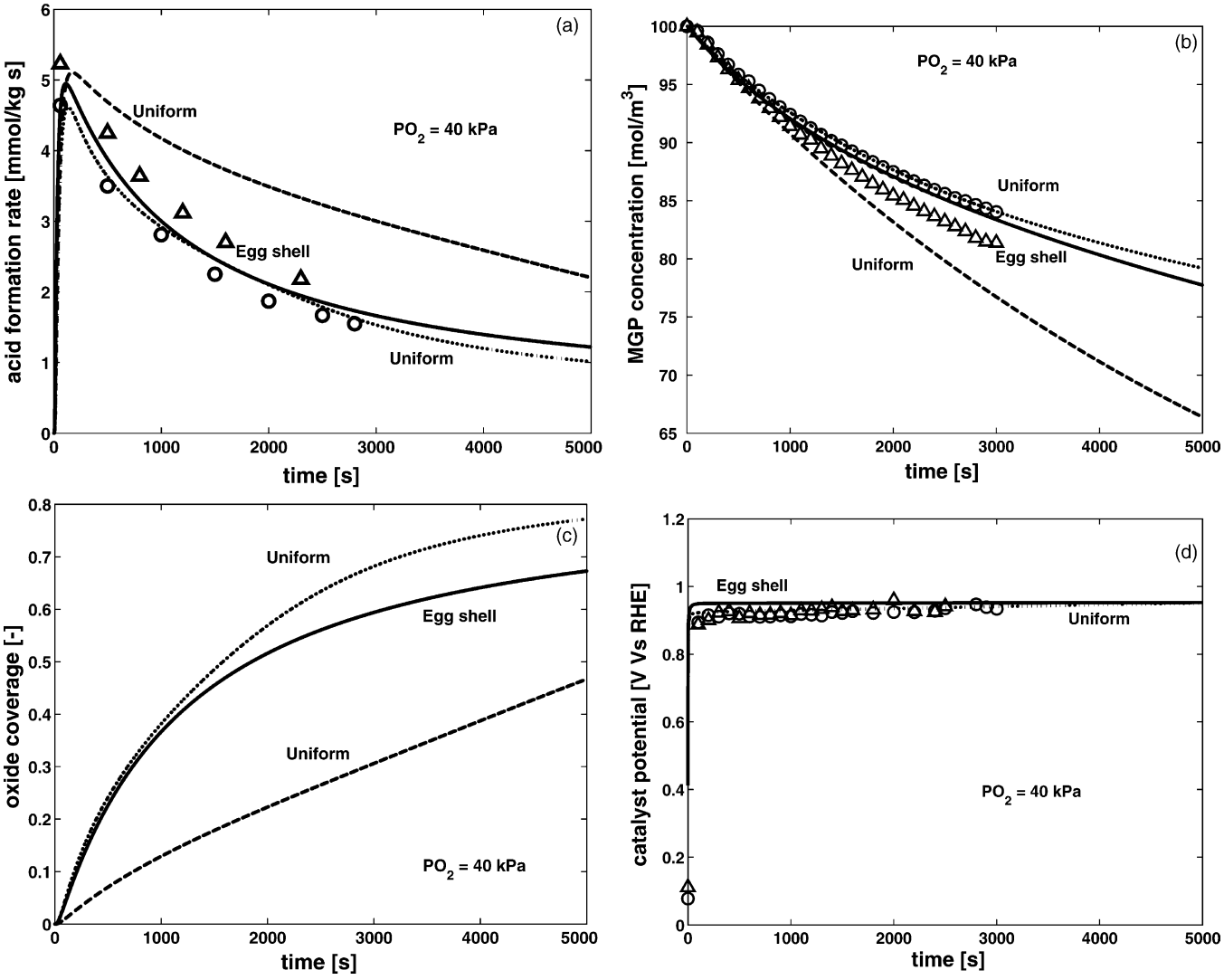

Fig. 4. MGP oxidation: the effect of a high oxygen partial pressure on the catalyst performance: (a) acid formation rate; (b) concentration of MGP; (c) fraction of the oxide coverage; and (d) in situ open-circuit catalyst potential. Symbols represent the experimental and continuous lines represent the modelling results. For the egg shell catalyst, triangles and solid lines are used, whereas for the uniform catalyst, circles, dashed line (with a k_6 value from Table 2), and dotted lines (with a five times higher k_6) are used.

Table 5. The results presented in Fig. 5a indicate a significant improvement in the model performance. The model is now able to describe the trend qualitatively and quantitatively, for both catalysts. Fig. 5b shows the change in glucose concentration as a function of time. It can be seen that the model with adopted mass transfer and diffusion parameters, describes the observed conversion to gluconic acid. The uniform catalyst gives 7% conversion after 1000 s, whereas the egg shell gives a slightly lower of 6%. Fig. 5c and 5d show oxide formation and catalyst potential as a function of time respectively. It can be seen that the oxide coverage is negligible, which is well reflected in the lower potential. However, the model predicts higher potential than the measured potential. This might be due to the fact that the model does not consider presence of adsorbed hydrogen species, which are expected to be present for an easily dehydrogenating agent like glucose [3].

4.2.2. Effect of higher oxygen partial pressure

Fig. 6a shows the acid formation rate as a function of time for the egg shell and the uniform catalyst at 100 kPa oxygen partial pressure. It can be seen that increasing oxygen partial pressure from 5 kPa (Fig. 5a) to 100 kPa (Fig. 6a) the initial rate of acid formation for both catalysts becomes almost 8 times higher. However, the rate of catalyst deactivation due to over-oxidation is also fast. It can also be seen that both catalysts show similar behaviour and activity. The simulation results presented in Fig. 6a, indicate a large influence of the effective diffusivity or distribution coefficient, and possible particle-bubble interaction. Fig. 6b shows that the model describes the experimental rates till 25% conversion. For higher conversions the reaction rate is slightly overestimated for both catalysts. Fig. 6c and d show oxide formation and catalyst potential as a function of time respectively. At the beginning, the measured potential is

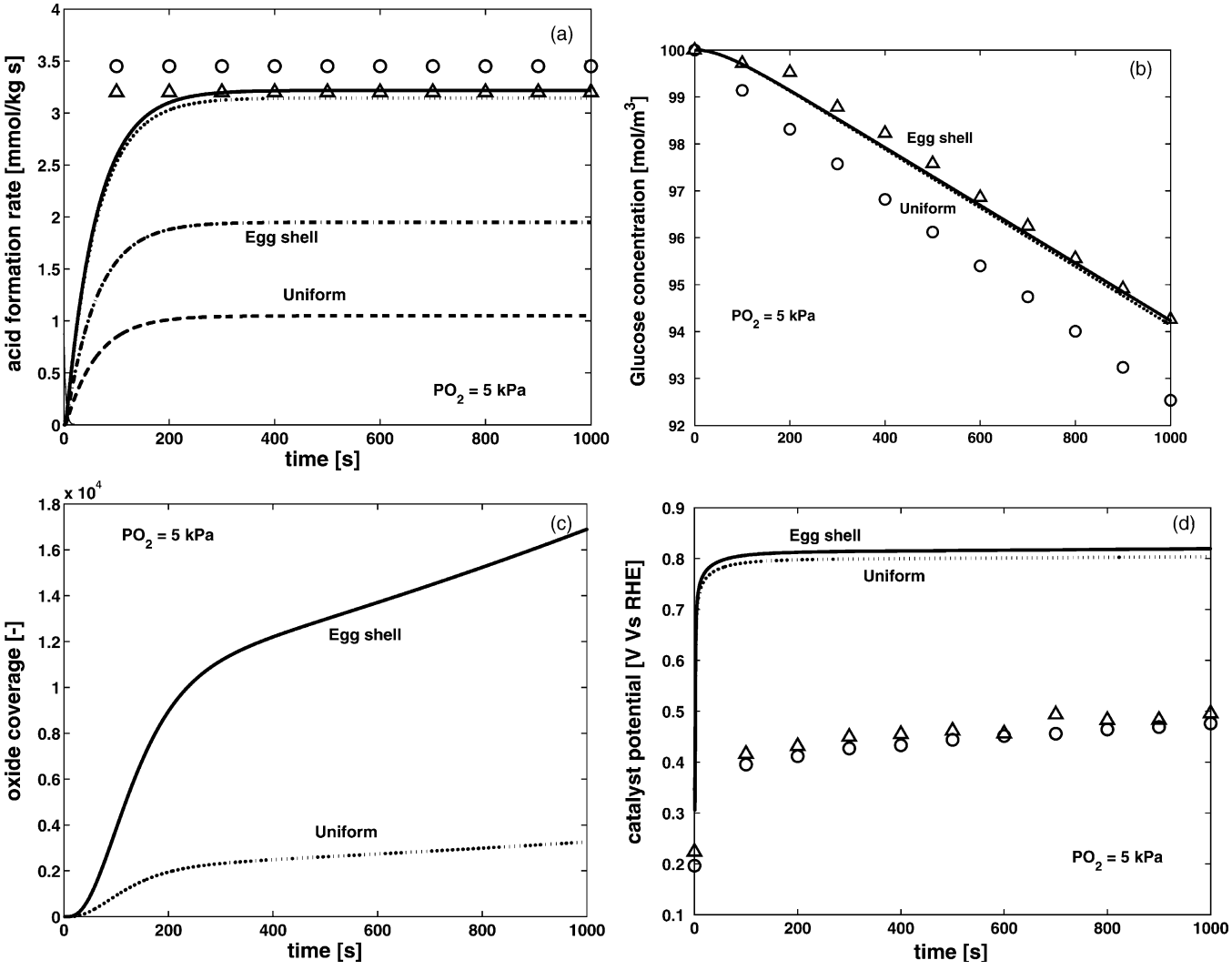

Fig. 5. Glucose oxidation: the effect of a low oxygen partial pressure on the catalyst performance: (a) acid formation rate, (b) concentration of glucose, (c) fraction of the oxide coverage, and (d) in situ open-circuit catalyst potential. Symbols represent the experimental and continuous lines represent the modelling results. For the egg shell catalyst, triangles, dash-dot line (with a values from Table 5), and solid lines (with a ten times higher D_{eff}, $k_{\text{GL,O}_2}a_{\text{GL,O}_2}$, and $k_{\text{LS,O}_2}$) are used, whereas for the uniform catalyst, circles, dashed line (with a values from Table 5) and dotted lines (with a 10 times higher D_{eff}, $k_{GL,O_2}a_{GL,O_2}$, and $k_{\text{LS,O}_2}$) are used.

irregular, possibly due to the presence of an easily dehydrogenating agent and pure oxygen gas. Only after some deactivation by over-oxidation the reading becomes stable and agrees with the simulated response.

5. Concluding remarks

In a semi-batch stirred reactor, the reaction rate of methyl glucoside (MGP) oxidation at oxygen partial pressure below 40 kPa, is found to be higher for the egg shell activity distribution than for the uniform catalyst activity distribution. Also, the deactivation rate due to over-oxidation increased dramatically with increasing oxygen partial pressure from 10 to 40 kPa, for both catalysts. For glucose, which has a higher rate of dehydrogenation, experimentally it is found that both catalysts give the same oxidation rate for all investigated oxygen partial pressures (5–100 kPa). Also, the rate of oxidation was five to eight times higher than the MGP oxidation rate. The developed reaction-engineering model is able to describe the observed experimental data for both catalysts. It is found that for the uniform catalyst, which has a small Pt particle size (higher dispersion), increasing the Pt–oxygen bonding, improved the model performance, especially for methyl glucoside oxidation. It is also found that glucose oxidation can only be modelled by considering that the reaction is taking place at the gas–liquid interface and is influenced by particle-bubble adhesion. For proper modelling good estimates for the effective diffusivity (D_{eff}) and partition coefficient (m) should be obtained, and the effect of PBA on mass transfer enhancement should be assessed.

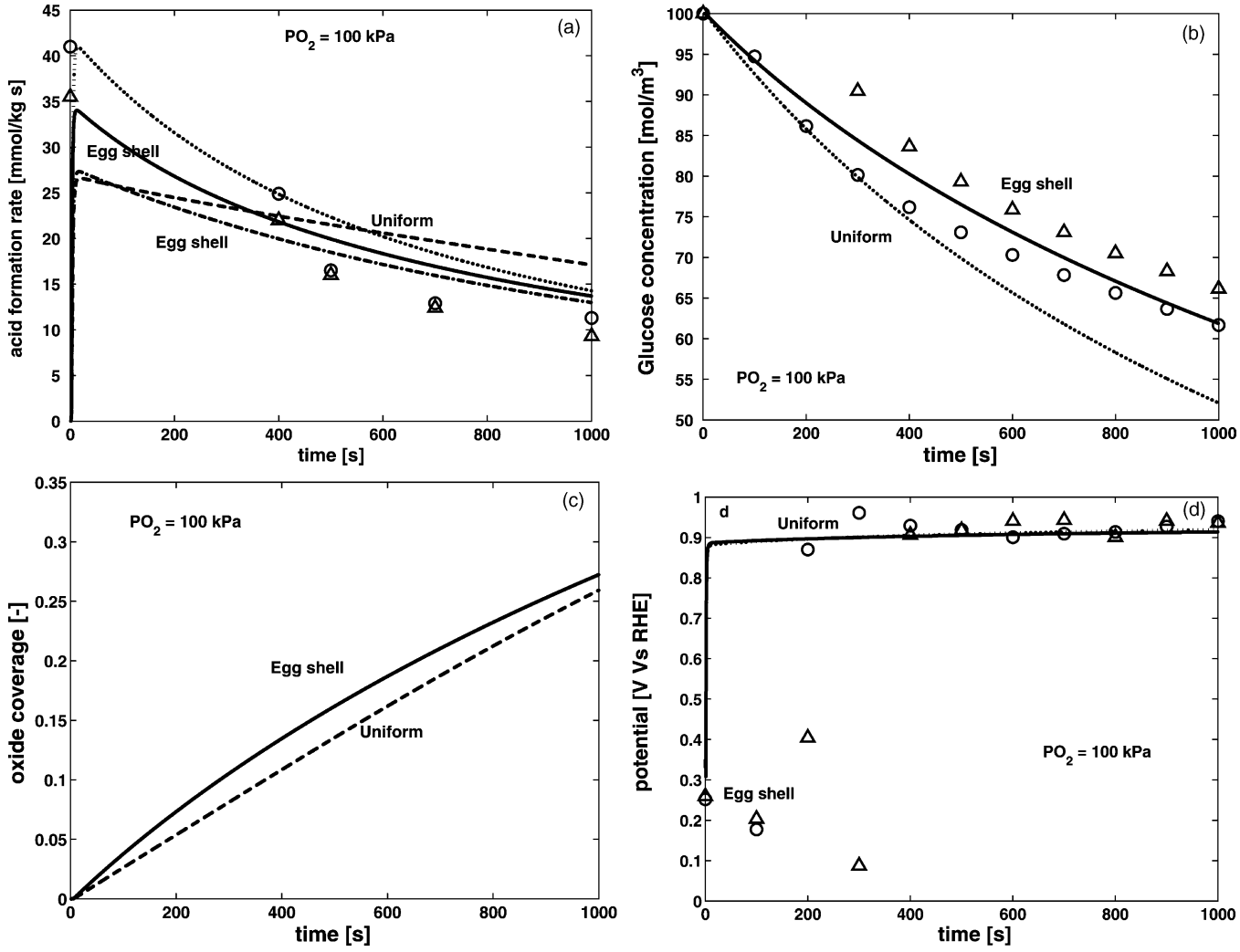

Fig. 6. Glucose oxidation: the effect of a high oxygen partial pressure on the catalyst performance. Symbols represent the experimental and continuous lines represent the modelling results. For the egg shell catalyst, triangles, dash-dot line (with a values from Table 5), and solid lines (with a 10 times higher D_{eff}, $k_{\text{GL,O}_2} a_{\text{GL,O}_2}$, and $k_{\text{LS,O}_2}$) are used, whereas for the uniform catalyst, circles, dashed line (with a values from Table 5) and dotted lines (with a 10 times higher D_{eff}, $k_{\text{GL,O}_2} a_{\text{GL,O}_2}$, and $k_{\text{LS,O}_2}$) are used.

The catalyst potential measurement and its subsequent modelling are proven to be accurate for low reducing compounds. However, for high reducing compounds, in the presence of pure oxygen gas, potential measurement is instable and the measuring technique needs to be improved. Also, the electrochemical kinetic model has to be improved by taking into account adsorbed hydrogen species and additional electro active reaction of proton formation.

In this work it is shown through modelling, that Pt particle size (dispersion) has a strong effect for a low reducing compound like methyl glucoside (MGP). However, this effect needs to be scrutinized via experiments, using more catalysts with different dispersion. Also, the effect of support needs to be investigated, along with possible limitations for the active sites accessibility for the alcohol molecule. The model can be further improved by taking into consideration of diffusion limitation for the alcohol molecule, which can be crucial at higher conversion.

References

[1] T. Mallat, A. Baiker, Oxidation of alcohols with molecular oxygen on platinum metal catalysts in aqueous solutions, Catal. Today 19 (1994) 247–284.
[2] P. Gallezot, Selective oxidation with air on metal catalysts, Catal. Today 37 (1997) 405–418.
[3] J.H.J. Kluytmans, A.P. Markusse, B.F.M. Kuster, G.B. Marin, J.C. Schouten, Engineering aspects of the aqueous noble metal catalysed alcohol oxidation, Catal. Today 57 (2000) 143–155.
[4] J.H. Vleeming, B.F.M. Kuster, G.B. Marin, Selective oxidation of methyl α-D-glucopyranoside with oxygen over supported platinum: kinetic modeling in the presence of deactivation by overoxidation of the catalyst, Ind. Eng. Chem. Res. 36 (1997) 3541–3553.
[5] B. Beden, J.M. Leger, C. Lamy, in: J. O'M. Bockris, B. E. Conway, R.E. White (Eds.), Modern Aspects of Electrochemistry, vol. 22, Elsevier, Amsterdam, 1992, p. 97.
[6] E. Pastor, S. Wasmus, T. Iwasita, M.C. Arvalo, S. Gonzlez, A.J. Arvia, Spectroscopic investigations of c3 primary alcohols on platinum electrodes in acid solutions. Part I. *n*-Propanol, J. Electroanal. Chem. 350 (1) (1993).

[7] G. Horanyi, Heterogeneous catalysis and electrocatalysis, Catal. Today 19 (1994) 285–312.
[8] A.P. Markusse, B.F.M. Kuster, J.C. Schouten, Platinum catalysed aqueous methyl α-D-glucopyranoside oxidation in a multiphase redox-cycle reactor, Catal. Today 66 (2001) 191–197.
[9] V.R. Gangwal, B.G.M. van Wachem, B.F.M. Kuster, J.C. Schouten, Platinum catalysed aqueous alcohol oxidation: model based investigation of reaction conditions and catalyst design, Chem. Eng. Sci. 57 (2002) 5051–5063.
[10] V.R. Gangwal, J. van der Schaaf, B.F.M. Kuster, J.C. Schouten, The effect of mass transport limitation on the estimation of intrinsic kinetic parameters for negative order reactions. Appl. Catal. A: Gen. (2004), in press.
[11] Y. Schuurman, B.F.M. Kuster, K. van der Wiele, G.B. Marin, Selective oxidation of methyl α-D-glucoside on carbon supported platinum. Part II. Assessment of the arrhenius and langmuir parameters, Appl. Catal. A: Gen. 25 (1992) 31–46.
[12] J.H. Vleeming, B.F.M. Kuster, G.B. Marin, Oxidation of methyl and *n*-octyl α-D-glucopyranoside over graphite-supported platinum catalysts: effect of alkyl substituent on activity and selectivity, Carbohydrate Res. 303 (1997) 175–183.
[13] J.H. Vleeming, B.F.M. Kuster, G.B. Marin, Effect of platinum particle size and catalyst support on the platinum catalysed selective oxidation of carbohydrates, Catal. Lett. 46 (1997) 187–194.
[14] P. Vinke, W. van der Poel, H. van Bekkum, On the oxygen tolerance of noble metal catalysts in liquid phase alcohol oxidations: the influence of the support on catalyst deactivation. Studies in Surface Science and Catalysis, Elsevier, Amsterdam, 1991.
[15] T. Mallat, A. Baiker, Catalyst potential: a key for controlling alcohol oxidation in multiphase reactors, Catal. Today 24 (1995) 143–150.
[16] T. Mallat, A. Baiker, Catalyst potential measurement: a valuable tool for understanding and controlling liquid phase redox reactions, Top. Catal. 8 (1999) 115–124.
[17] F. Parmigiani, E. Kay, P.S. Bagus, Anomalous oxidation of platinum clusters studied by X-ray photoelectron spectroscopy, J. Electron Spectrosc. Related Phenom. 50 (1990) 39–46.
[18] H.E. van Dam, H. van Bekkum, A note on stabilized Pt/C oxidation catalysts: Absence of gas–liquid boundary deactivation results in relatively high efficiency (Pt/C oxidation catalysts; Part 6), React. Kinet. Catal. Lett. 40 (1) (1989) 13–17.
[19] E. Alper, B. Wichtendahl, W.D. Deckwer, Gas absorption mechnism in catalytic slurry reactors, Chem. Eng. Sci. 35 (1980) 217–222.
[20] M. van der Zon, H. Thoolen, P.J. Hamersma, E.K. Poels, A. Bliek, Agglomeration and adhesion of catalyst particles in gas–liquid reactors, Catal. Today 66 (2001) 263–270.
[21] R.H. Perry, D. Green, J.O. Maloney, Perry's Chemical Engineers' Handbook, McGraw-Hill, New York, 1997.
[22] W. Groenland, Gas-to-Liquid Mass Transfer Coefficient Measurements, Internal Report, 2003.
[23] Y. Sano, N. Yamaguchi, T. Adachi, Mass transfer coefficients for suspended particles in agitated vessels and bubble columns, J. Chem. Eng. Jpn. 7 (1974) 255–261.